Ocean Engineering 340 (2025) 122327

Contents lists available at ScienceDirect

Ocean Engineering

journal homepage: www.elsevier.com/locate/oceaneng

Research paper

Aerodynamic damping in decoupled dynamic modeling of floating offshore wind turbines

Yanfei Deng [a], Sara Ying Zhang [b], Yifeng Yang [c,*], Bingfu Zhang [a], Yifei Wang [a], Jiahao Chen [d], Weiping Hou [e]

[a] School of Intelligence, Harbin Institute of Technology Shenzhen, Shenzhen, 518000, Guangdong, China
[b] School of Electromechanical Engineering, Guangdong University of Technology, Guangzhou, 510000, Guangdong, China
[c] Department of Mechanical Engineering, University College London, Torrington Place, London, WC1E 7JE, United Kingdom
[d] School of Ocean Engineering and Technology, Sun Yat-sen University, Zhuhai, 519000, Guangdong, China
[e] CIMC Offshore Co. Ltd, 4008 Menghai Avenue, Qianhai Shenzhen-Hong Kong Cooperation Zone, 518000, Shenzhen, China

ARTICLE INFO

Keywords:
Decoupled model
Motion response
Floating offshore wind turbine
Aerodynamic damping

ABSTRACT

Accurate and efficient modeling of floating offshore wind turbines (FOWTs) is crucial for fast iteration and optimization of design solutions. However, the commonly used coupled models are normally time-consuming, data intensive, and hard to satisfy the requirement of fast prediction of environmental loads. By contrast, efficient decoupling methods of FOWTs are still insufficiently accurate and require further investigation. As a result, this paper focuses on the effects of aerodynamic damping on the prediction accuracy in decoupled simulations. Firstly, an aerodynamic model is established for the referenced wind turbine, which is used to identify both the constant and frequency-dependent aerodynamic coefficients. Subsequently, decoupled models are developed for the referenced FOWT by treating the aerodynamic thrust forces as concentrated loads, incorporating aerodynamic damping and added mass as 'additional' components of the original hydrodynamic coefficients. By comparing the surge and pitch responses between the decoupled and coupled models, the role and applicability of aerodynamic damping in decoupled models are demonstrated. Our findings highlight the substantial influence of the frequency-dependent characteristics of aerodynamic damping on the decoupled analyses, offering valuable insights for the establishment of efficient and accurate decoupled models in practical engineering design.

1. Introduction

The substantial utilization of wind energy in shallow seas has driven the development of floating offshore wind turbines (FOWTs) as a promising solution for harnessing wind energy in deeper and more remote marine environments. However, the high levelized cost of energy (LCOE) remains a major challenge for the wide deployment of FOWTs (Ghigo et al., 2020). To reduce costs associated with FOWTs, innovative design, optimization, advanced supply chain management, and structural modularity are key factors (Foxwell, 2022; Riyanto et al., 2022). Hence, one of the crucial tasks is to develop accurate and efficient simulation hydrodynamic and aerodynamic tools for FOWTs.

FOWTs are inherently complex multi-body systems with noticeable trans-stiffness properties, which makes the aero-hydrodynamic coupling a pivotal concern in its dynamic analysis (Souza et al., 2020). The existing standards uniformly require the consideration of combined wind-wave-current loads and internal coupling interactions among substructures for FOWT dynamics (DNV·GL, 2018a; IEC, 2019).The present prevailing approach is called nonlinear aero-hydro-servo-elastic time-domain analysis. In particular, the aerodynamic loads are evaluated by the iterative blade element momentum (BEM) method. The added mass, linear damping, and wave force transfer functions are obtained from a comprehensive three-dimensional diffraction model or the Morison model, depending on the sizes of the structures. The mooring loads can be calculated using a series of methods, such as the quasi-static approach, lumped mass models, or finite element methods (Subbulakshmi et al., 2022). Coupled numerical simulations employing codes like FAST, OrcaFlex, and Bladed have been validated against wave tank model tests, demonstrating the ability of the aero-hydro-servo-elastic time-domain analysis approach to appropriately address coupling effects among substructures and external excitations (Chuang et al., 2021; Jonkman, 2007; Subbulakshmi et al., 2022;

* Corresponding author.
E-mail address: yifeng.yang.19@ucl.ac.uk (Y. Yang).

https://doi.org/10.1016/j.oceaneng.2025.122327
Received 8 February 2025; Received in revised form 18 June 2025; Accepted 27 July 2025

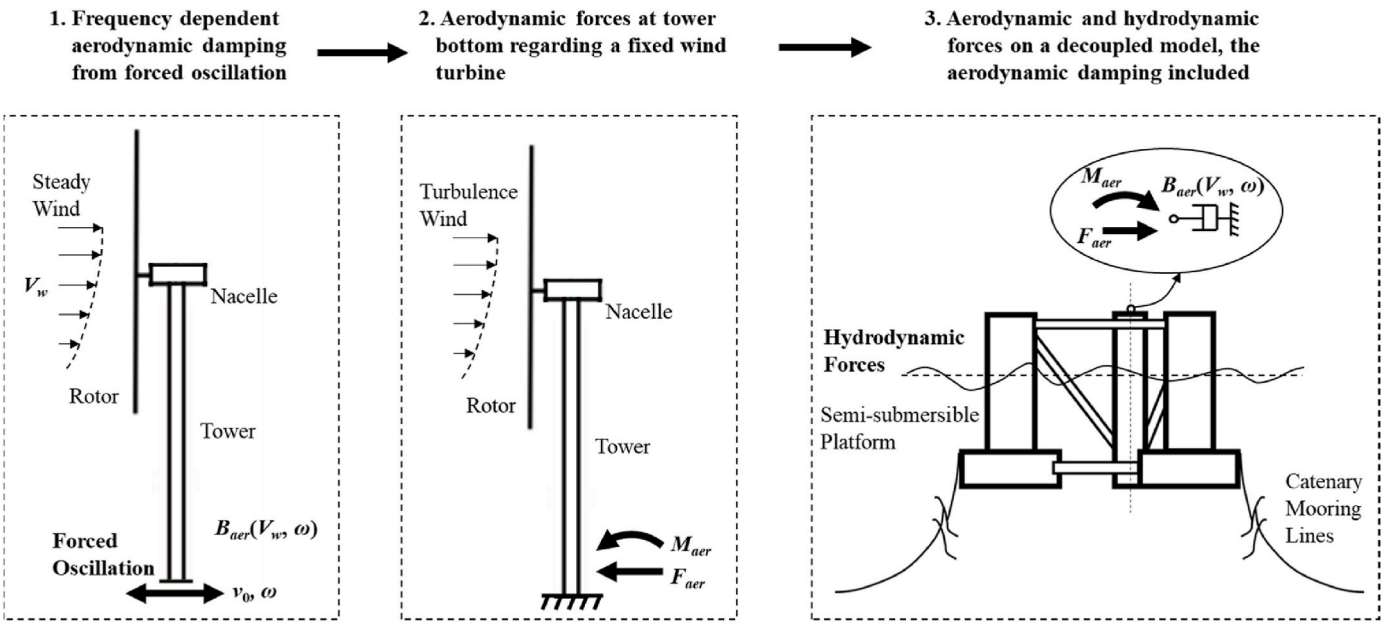

Fig. 1. Schematization of the decoupling approach.

Yang et al., 2021).

Although aero-hydro-servo-elastic coupled models have been widely used in a series of research e.g. (Ma et al., 2022; Yang et al., 2020), their practical application in practical design remains limited. This can be attributed to two central factors. First, the design process of FOWTs requires the consideration of thousands of design load cases. Conducting coupled time-domain analyses for these cases can be highly time-intensive and resource-draining. Second, wind turbines and floating foundations are typically designed independently, with turbine manufacturers and foundation designers operating separately and often keeping design details confidential. In contrast, a simplified or decoupled dynamic model may offer a more practical solution, where the system's degrees of freedom are reduced, and the computational efficiency is significantly enhanced. Additionally, such methods also capitalize on existing subsystem knowledge, thus bolstering accuracy and credibility in design processes.

In the design of floating foundations and mooring systems, a common and simplified approach involves the consolidation of the mass of the rotor-nacelle-assembly (RNA) at the tower top, with the resultant aerodynamic loads applied. For instance, Karimirad and Moan (2012) developed a simplified aero-hydrodynamic model using the Simo-Riflex package, which incorporated a dynamic link library (DLL) referred to as "TDHMILL" to provide aerodynamic loads. The controller was simplified into a filter to eliminate negative damping by removing velocity components associated with frequencies close to the natural frequency of pitch. Matha et al. (2014) developed a reduced nonlinear model with simplified hydrodynamic and aerodynamic formulas. Aerodynamic loads were represented as torque and thrust forces on the shaft, determined by tip speed ratio and rotor azimuth angle. Furthermore, Lerch et al. (2018) presented a simplified model for the dynamic analysis and power generation of a FOWT. In their model, aerodynamic loads were estimated approximately based on a thrust coefficient formula associated with wind speeds. Beshbichi et al. (2021) introduced an innovative, object-oriented approach to model the dynamic response of FOWTs within the Modelica environment. In their approach, aerodynamic loads were calculated by mapping steady-state aerodynamic coefficients, and a rotor-collective blade-pitch control model was implemented.

An alternative approach uses pre-calculated aerodynamic thrust forces and incorporates aerodynamic damping related to the nacelle motion, achieving aero-hydrodynamic decoupling. This method has been widely studied, particularly in the context of fixed wind turbines. For instance, Xi et al. (2020) and Valamanesh and Myers (2014) have derived semi-analytical and analytical solutions for wind turbine aerodynamic damping based on the BEM theory, and applying them to decouple the seismic response analyses of fixed wind turbines. Chen et al. (2021) proposed an efficient model for fatigue analysis of monopile-supported offshore wind turbines, relying on an aerodynamic decoupling strategy combined with modal reduction techniques. Chen et al. (2020) incorporated a coupled aerodynamic damping matrix into a finite element model to evaluate tower vibration responses. Rixen and Valk (2013) introduced a substructure method based on impulse response functions and employed it in the time-domain analysis of offshore wind turbines located on jacket foundations. For FOWTs, Alexandre et al. (2021) developed a simplified aerodynamic load model based on drag and lift coefficients, in which the aerodynamic loads are estimated as a function of the angle between the rotor and the wind direction, achieving calculation errors within a margin of 4 %. These advancements demonstrate that decoupled time-domain analysis is an efficient tool for FOWT design.

Compared to fixed wind turbines, FOWTs experience more significant fore-aft motion and have additional degrees of freedom in motion. Pegalajar-Jurado et al. (2018) presented an efficient frequency-domain model of FOWTs by extracting the aerodynamic damping from decay tests specific for four planar degrees of freedom. Souza and Bachynski (2019) found that the relative phase between the nacelle velocity and the thrust leads to an apparent inertia/damping effect, which is tightly related to the variations of pitch decay period. Later, Souza et al. (2020) developed an efficient approach to evaluate the frequency-domain responses of FOWTs using frequency-dependent damping and inertia terms. Most recently, Deng et al. (2023) investigated how the frequency-dependent characteristics of aerodynamic damping influence the dynamic responses of a FOWT. Nevertheless, research specific to time-domain decoupled methodologies for FOWTs is relatively limited, and the effects of different aerodynamic damping on the performance of decoupled models under diverse operational conditions have received little attention.

To sum up, while the reliability of coupled simulations for floating wind turbines is well established, research on decoupled analysis remains largely confined to frequency-domain approaches and time-domain studies under parked conditions. This paper proposes three key contributions. First, an efficient time-domain decoupled approach for the dynamic analysis of FOWTs is presented. Second, the effects of

different aerodynamic damping on the performance of decoupled models are fully revealed. Third, the results demonstrate the importance of including frequency-dependent aerodynamic damping in decoupled analyses of FOWTs.

The remainder part of the paper is organized as follows. In Section 2, the decoupling approach, the model configuration and the reference NREL 5 MW wind turbine used in this study are presented. The aerodynamic and hydrodynamic damping are evaluated and discussed in Section 3. In Section 4, analysis and comparison are conducted for the results of motion responses under different damping schemes evaluated from the decoupled and coupled models. Followed by the conclusion and practical selection suggestions for aerodynamic damping in decoupled modeling of FOWTs.

2. Methodology and modeling

For comparison, we established a coupled aero-hydro-servo-elastic model and a decoupled model for aerodynamic calculations using the established offshore engineering software, Orcaflex. The Orcaflex has a well-documented history of integration with the FAST software, and its accuracy and stability have been validated (Yang et al., 2022).

2.1. Decoupling approach

In this study, different from the conventional coupled model, the decoupled model takes a distinct approach to addressing aerodynamic loads. In the coupled model, the calculation of aerodynamic forces on the rotor should be based on real-time relative wind speed, and these forces serve as excitation forces influencing the dynamic response of the system. In contrast, the decoupled model characterizes the fluctuation in the aerodynamic force due to the rotor motion as frequency-dependent inertia and damping effects. Consequently, the aerodynamic force is divided into three components: the added mass force, the damping force, and the excitation force.

As illustrated in Fig. 1, the aerodynamic damping and added mass of the wind turbine at various wind speeds need to be identified as a preliminary step. Furthermore, pre-calculation of aerodynamic excitation forces for the fixed wind turbine under specific wind conditions is essential. In this study, we choose the tower base as the interface bridging the aerodynamic model and the hydrodynamic models. Using the present decoupled model, the aerodynamic excitation forces, in conjunction with the effects of aerodynamic damping and added mass, are assumed to be applied at the interface point on the tower base. This is considered to combine with a hydrodynamic model for the floating platform and mooring system.

A key problem here to achieve high-accuracy computation is the accurate prediction of the aerodynamic damping matrix B_{aer}, which is typically obtained by the partial derivative of the aerodynamic thrust F^T with respect to the inflow wind speed V_w. Here, it is approximated by a first-order forward finite difference scheme, which provides

$$b_{aer}(V_w) = \frac{\partial F^T(V_w)}{\partial V_w} \approx \frac{F^T(V_w + \Delta V_w) - F^T(V_w)}{\Delta V_w} \tag{1}$$

Eq. (1) cannot account for dynamic servo effects associated with blade pitch control. To identify frequency-dependent aerodynamic damping and reveal how the motion frequencies of a FOWT influence aerodynamic damping, the common forced oscillation approach can be adopted. When employing an oscillating rotor, the rotor fore-aft velocity $\dot{x}$ and the thrust force F^T can be expressed as

$$\begin{aligned} \dot{x} &= v_0 \cos(\omega t) \\ F^T &= F^T_{ave} + F^T_{osc} \end{aligned} \tag{2}$$

where F^T_{ave} and F^T_{osc} represent the averaged and oscillatory components F^T, v_0 denotes the forced oscillation velocity of the turbine, ω denotes the corresponding oscillatory frequency, t denotes the time. The oscillatory component can be represented as the sum of added mass and damping forces, as follows.

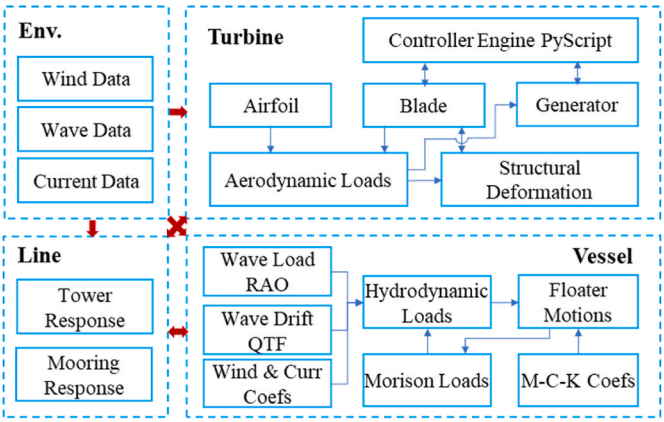

Fig. 2. Schematic diagram of Orcaflex framework.

$$F^T_{osc} = f_0 v_0 \cos(\omega t + \alpha) = f_0 \cos(\alpha)\dot{x} + \frac{f_0 \sin(\alpha)}{\omega}\ddot{x} = -a_{aer}\ddot{x} - b_{aer}\dot{x}, \tag{3}$$

where f_0 represents response amplitude operator, α denotes the phase angle. Then, the aerodynamic added mass a_{ber} and damping b_{aer} of the wind turbine can be determined using the formula below.

$$a_{aer}(V_w, \omega) = \frac{1}{\omega v_0}\frac{2}{N}\sum_{i=1}^{N} F^T_{osc}(t_i) sin(\omega t_i), \tag{4}$$

$$b_{aer}(V_w, \omega) = -\frac{1}{v_0}\frac{2}{N}\sum_{i=1}^{N} F^T_{osc}(t_i) cos(\omega t_i), \tag{5}$$

where N represents the number of time points considered.

We may define the following aerodynamic matrices of added mass and damping, i.e., A_{aer} and $B_{aer,}$ which are applied to the hydrodynamic coefficient matrices as additional terms for added mass or damping later.

$$\begin{aligned} A_{aer}(\omega) &= \begin{bmatrix} a_{aer}(\omega) & 0 & a_{aer}(\omega) z_{hub} \\ 0 & 0 & 0 \\ a_{aer}(\omega) z_{hub} & 0 & a_{aer}(\omega) z^2_{hub} \end{bmatrix}, \\ B_{aer}(\omega) &= \begin{bmatrix} b_{aer}(\omega) & 0 & b_{aer}(\omega) z_{hub} \\ 0 & 0 & 0 \\ b_{aer}(\omega) z_{hub} & 0 & b_{aer}(\omega) z^2_{hub} \end{bmatrix}, \end{aligned} \tag{6}$$

where z_{hub} is the height of hub center.

In this study, for the sake of simplicity, the uniform steady-state inflow wind was considered in deriving the aerodynamic added mass and damping coefficients. The blade pitch angle and rotor speed were allowed to vary dynamically with the relative wind speed.

2.2. Orcaflex model

The FOWT is a complex muti-body coupling system. OrcaFlex provides a wide range of objects to model the various components of the wind turbine system, as illustrated in Fig. 2.

In this study, the RNA is modeled using the "Turbine" object, which utilizes the BEM method to estimate aerodynamic loads. The floater is represented as a 6-degrees-of-freedom (DOF) rigid body. This study employs a hybrid modeling approach for floater hydrodynamics, combining potential flow diffraction theory with Morison equation formulations. This methodology simultaneously resolves diffraction effects and viscous contributions. The tower structure and mooring system are both simplified using "line" objects. By contrast, the "Turbine" and

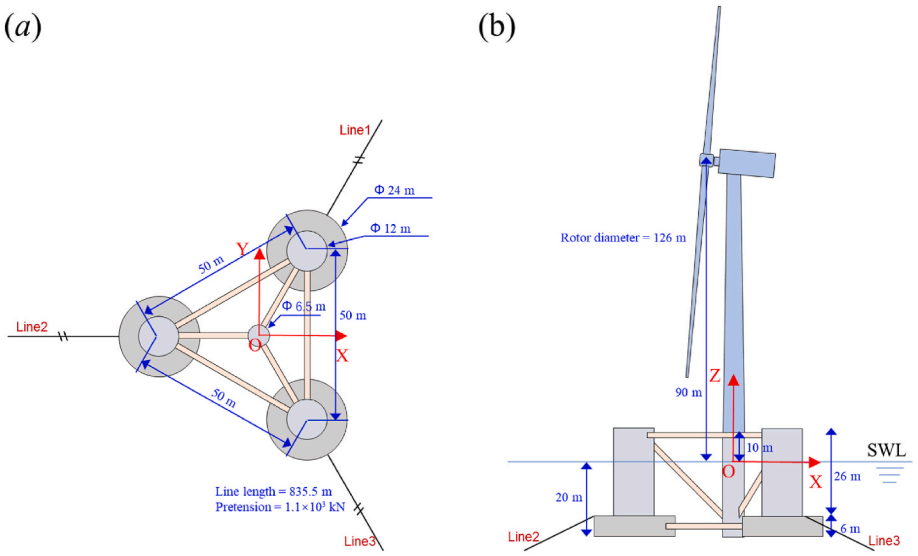

Fig. 3. Coordinate system definition and main dimensions of the reference semi-submersible. (a) Top view; (b) Side view.

"Vessel" objects are modeled as nodes. The "Line" objects are segmented into multiple elements, which are interconnected with the nodes to form each component of the wind turbine system. The motion equations governing the rigid body and the nodes can be expressed as

$$M(p,a)+C(p,v)+K(p)=F(p,v,t) \tag{7}$$

where $M(p,a)$ represents the system inertia load, $C(p,v)$ represents the system damping load, $K(p)$ represents the system stiffness load, and $F(p,v,t)$ represents the external loads, primarily including wave excitation, Morison drag force, aerodynamic force. $\boldsymbol{p}$, $\boldsymbol{v}$, and $\boldsymbol{a}$ denote the position, velocity, and acceleration vectors, respectively, and t represents the simulation time.

The wind turbine is simulated in both the coupled model and the aerodynamic model to calculate excitation forces and damping. The blade DOFs remain unconstrained to account for aeroelastic coupling effects. Each blade is discretized into 17 segments, allowing for the integration of aerodynamic and structural forces. A conventional variable-speed, variable blade-pitch-to-feather control configuration (Robertson et al., 2014) are implemented via external Python scripts to represent various operating conditions. The Prandtl tip and hub loss, and Pitt and Peters skewed wave corrections are included in the aerodynamic models.

The hydrodynamic coefficients of the floater, including the hydrostatic stiffness, added mass, linear damping, transfer functions for 1st-order wave forces and wave drift forces, are imported from OrcaWave model. Morison elements were created for each submerged component of the floater and additional damping were introduced to match the damping level of model tests. This ensures hydrodynamic damping fidelity, which is a prerequisite for isolating aerodynamic damping effects and contributions in coupled dynamic analysis. Tabel 1 presents the Morison drag coefficients and additional linear and quadratic damping.

To optimize computational efficiency, an implicit integration scheme is applied with a 0.1s time step and a total simulation time of 10,800 s.

2.3. Reference wind turbine

The reference wind turbine employed in this study consists of a OC4 DeepCWind platform and a NREL 5 MW wind turbine. The platform features a catenary-moored semi-submersible configuration, as sketched in Fig. 3. The DeepCWind semi-submersible platform comprises a central column and three outer columns, with a large-diameter bottom column attached to each of the outer columns to increase the added mass and damping of the floater. The mooring system employed is a three-point catenary configuration, adapted to a water depth of 200 m. A three-blade 5 MW wind turbine is located atop the center column. The tower base is situated 10.0 m above the still water level (SWL), and the hub center is at an elevation of 90.0 m. The cut-in, rated and cut-out wind speeds of the turbine are 3 m/s, 11.4 m/s, and 25.0 m/s, respectively. Please refer to Robertson et al. (2014) for further details regarding the floating foundation and the turbine unit.

2.4. Met-ocean conditions

This study conducts time-domain simulations with random irregular waves and turbulent winds to thoroughly evaluate the effectiveness of the decoupled approach in predicting dynamic responses under realistic sea states.

The JONSWAP spectrum, as defined in Tucker and Pitt (2001), is adopted here, which gives

$$S(f)=\frac{\alpha g^2}{16\pi^4}f^{-5}\exp\left[-\frac{5}{4}\left(\frac{f}{f_p}\right)^{-4}\right]\gamma^{\exp\left[-\frac{1}{2\sigma^2}\left(\frac{f}{f_p}-1\right)^2\right]} \tag{8}$$

where α is the spectral energy parameter, g is the acceleration due to gravity, f is the wave frequency, and the bandwidth parameter σ is defined as

$$\sigma=\begin{cases}0.07 & for\ f\le f_p\\ 0.09 & for\ f\succ f_p\end{cases} \tag{9}$$

and the f_p denotes the peak spectral frequency, γ is the peak enhancement factor.

The IEC Kaimal model is employed for simulating wind conditions. The spectra for the three wind components, represented as $K=u, v, w$, are given by

Table 1
Morison drag coefficients and additional damping for floater structure.

Normal drag coefficient	Axial drag coefficient	Additional linear damping	Additional quadratic damping
1.2	4.8 (base column)/ 0.0 (others)	70 kN/(m/s)	70 kN/(m/s)^2

Table 2
Sea state parameters for time-domain analyses.

Env.	Wave	Current	Wind	Note
Case A	$H_s = 2.02$ m, $T_p = 5.47$ s, $\gamma = 1.0$	$V_c = 0.18$ m/s	$V_w = 9.8$ m/s, $TI = 10.0$ %	Below-rated Wind Speed
Case B			$V_w = 11.4$ m/s, $TI = 14.6$ %	Rated Wind Speed
Case C			$V_w = 13.0$ m/s, $TI = 14.6$ %	Above-rated Wind Speed
Case D	$H_s = 6.9$ m, $T_p = 11.8$ s, $\gamma = 3.3$	$V_c = 0.84$ m/s	$V_w = 21.7$ m/s, $TI = 14.6$ %	Near-cut-out Wind Speed

Table 3
Natural periods derived from free-decay tests under still-water conditions.

DOF	Surge	Sway	Heave	Roll	Pitch	Yaw
Test (s)	107	112	17.5	26.9	26.8	82.3
Orcaflex (s)	113	113	17.7	25.7	25.7	78

$$S_K(f) = \frac{4\sigma_K^2 L_K/\overline{u}_{hub}}{(1+6fL_K/\overline{u}_{hub})^{5/3}}$$
$$L_K = \begin{cases} 8.10\Lambda_U, K = u \\ 2.70\Lambda_U, K = v \\ 0.66\Lambda_U, K = w \end{cases} \quad (10)$$
$$\sigma_K = \begin{cases} TI\cdot\overline{u}_{hub}, K = u \\ 0.8\cdot TI\cdot\overline{u}_{hub}, K = v \\ 0.5\cdot TI\cdot\overline{u}_{hub}, K = w \end{cases}$$

where f signifies the cyclic frequency, $\overline{u}_{hub}$ is the average wind speed at the hub height, TI represents the turbulence intensity, σ_K denotes the standard deviations of the velocity component k, L_K denotes an integral scale parameter, and Λ_U represents the turbulence scale parameter, typically selected as $0.7z_{\text{hub}}$ (see Table 1).

Table 2 provides an overview of the sea state parameters utilized for time-domain analyses. During the design phase, it is essential to verify various loading conditions in compliance with relevant standards (DNV·GL, 2018b). Among these, the normal operating condition represents the most frequently encountered state for FOWTs. In this case, the magnitude of aerodynamic damping for FOWTs is notably significant near rated wind speed. Its variation pattern is intricate, exerting a substantial influence on the system's dynamic responses. Therefore, this study examines three operating conditions near rated wind speed (9.8 m/s, 11.4 m/s, 13.0 m/s) and an additional operating condition near cut-out wind speed (21.7 m/s) for comparative analysis. The wave and current parameters correspond to the wind speed level, and the power-law exponent parameter is set as 0.14.

3. Hydrodynamic and aerodynamic damping

3.1. Free decay tests

Hydrodynamic and aerodynamic damping are both pivotal factors influencing the coupling dynamics of FOWTs. Accurately simulating hydrodynamic damping in FOWTs is a prerequisite for decoupled modeling. In this study, we refer to the model tests conducted by Coulling et al. (2013) to validate the natural periods and hydrodynamic damping obtained through free decay simulations under still-water conditions.

Table 3 presents a comparison of natural periods between numerical simulations and the model tests. It is clear to see that the natural periods of 6-dof directions are consistent between the tested and the simulation results except for the surge value. The discrepancy between surge natural periods results from the additional horizontal stiffness effects due to the cable bundle.

Fig. 4 presents the hydrodynamic damping ratio of the surge, heave, and pitch responses for both the results of OrcaFlex and the model tests, the ratio is calculated as

$$\mu = \frac{1}{2\pi}\ln\left|\frac{\phi_{An}}{\phi_{An+1}}\right|, \phi_{An} > \phi_{An+1} \quad (11)$$

where, ϕ_{An} and ϕ_{An+1} are the nth and n+1st peak values, respectively.

It can be found that the hydrodynamic damping shows clear nonlinear characteristics to the initial cycle amplitude. Furthermore, given the current model configuration, the hydrodynamic damping in the numerical model exhibits consistency with the model tests.

3.2. Aerodynamic added mass and damping

As previously mentioned, the initial phase of decoupled analysis involves the identification of aerodynamic damping and added mass. According to potential flow theory, the analytical solution for the added mass of an idealized disc undergoing infinite-period oscillations under fully submerged conditions is given by $m_{added} = \frac{8}{3}\rho R^3$. When applied to our turbine case by treating the rotor as an equivalent disc, this yields a constant added mass value of approximately 817 tonnes. However, that actual rotor behavior significantly deviates from this idealized model. The aerodynamics of wind turbine rotors are profoundly influenced by inflow wind speed, rotational speed, blade pitch angle, and oscillation frequency. Therefore, this study employs direct numerical simulation to

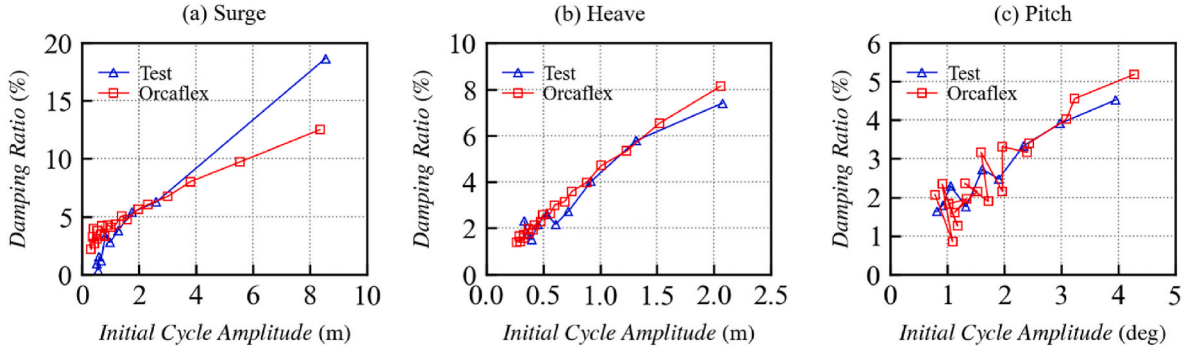

Fig. 4. Comparison of hydrodynamic damping from free-decay tests under still-water conditions: (a) Surge; (b) Heave; (c) Pitch.

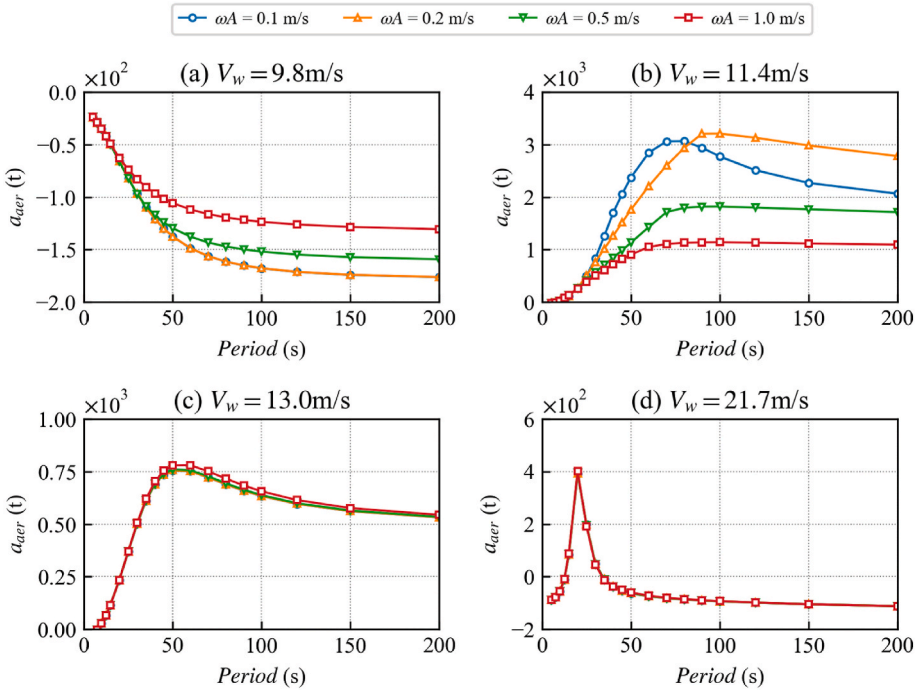

Fig. 5. Frequency-dependent aerodynamic added mass derived from fore-aft oscillation simulation.

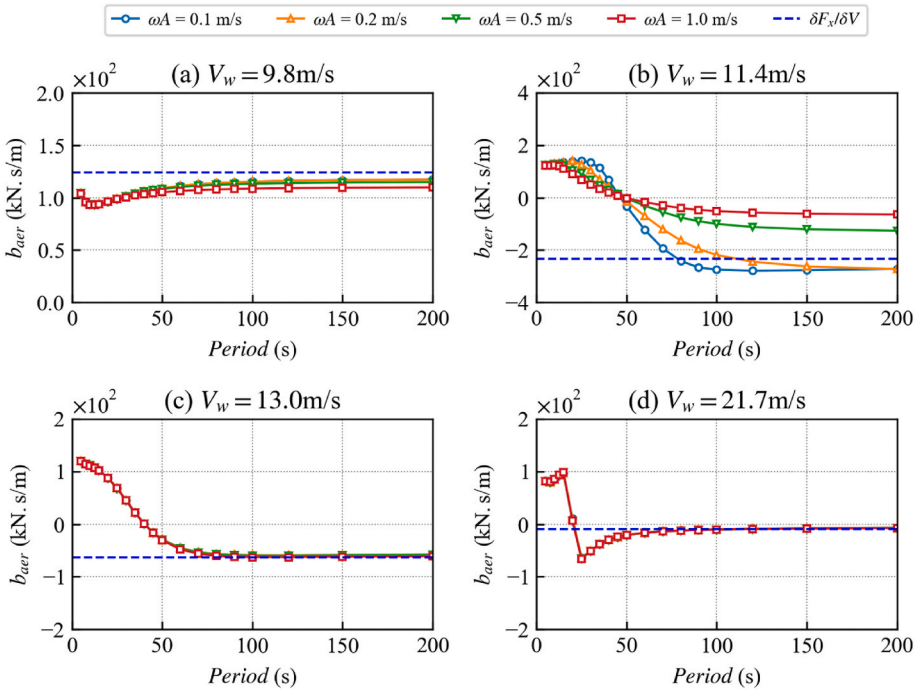

Fig. 6. Frequency-dependent aerodynamic damping derived from fore-aft oscillation simulation.

systematically identify the practical aerodynamic added mass and damping characteristics through forced reciprocating motion of the rotor across varying wind speeds. In this study, for constant damping, Eq. (1) considers a inflow wind speed interval or $\Delta V_w = 0.1$ m/ s. To capture the influences of nacelle velocity and turbulence wind, four oscillation velocities, namely $v_0 = 0.1\,\text{m/s}, 0.2\,\text{m/s}, 0.5\,\text{m/s}, 1.0\,\text{m/s}$ are considered. To simulate variations in relative wind speed, we directly modeled the rotor undergoing forced oscillation motion along the X-axis direction.

Fig. 5 presents the frequency-dependent aerodynamic added mass for the NREL 5 MW wind turbine. All mass values are reported in metric tonnes (t). The aerodynamic added mass remains relatively insignificant when the wind speed deviates considerably from the rated values (9.8 m/s, 21.7 m/s). However, as the wind speed approaches or crosses the rated wind speed (11.4 m/s, 13.0 m/s), the maximum value of aerodynamic added mass exhibits a substantial increase, potentially reaching magnitudes one order of magnitude higher than the RNA mass. This notable augmentation in aerodynamic added mass has the potential to exert a substantial influence on the natural periods of the FOWT and therefore demands careful consideration. Additionally, it is observed

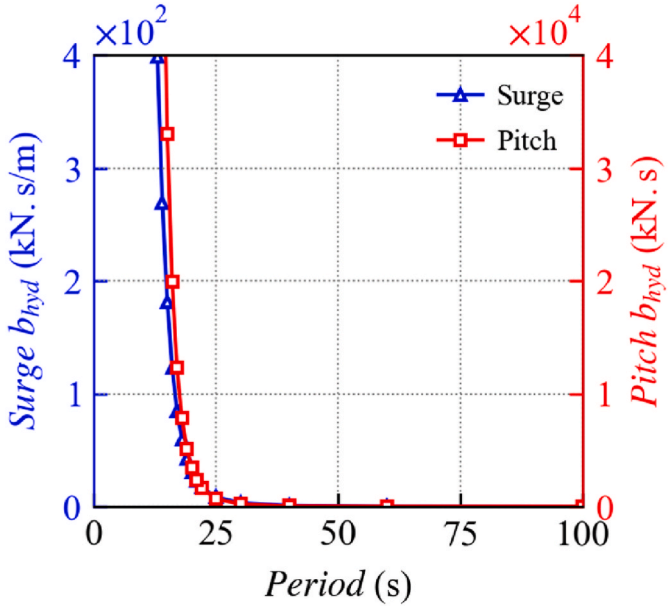

Fig. 7. Hydrodynamic damping imported from the diffraction model.

that at lower wind speeds (9.8 m/s, 11.4 m/s), the magnitude of the added mass exhibits a pronounced correlation with nacelle velocity. Particularly, the aerodynamic added mass reaches its zenith near the rated wind speed, ranging from approximately 1000 tons to 3000 tons. In comparison to the RNA mass, which amounts to 350 tons, the effect of added mass on the natural period of pitch response is significant and cannot be ignored.

Fig. 6 presents the outcomes concerning frequency-dependent aerodynamic damping. It can be seen that the variation of aerodynamic damping against the oscillatory periods is highly relevant to the wind speeds. A comparison between the damping value obtained from the difference scheme in Eq. (1) (blue dashed lines) is also compared with the results from the frequency simulation. It is observed that, with the increase of the oscillatory period, aerodynamic damping gradually tends to the constant damping value by Eq. (1). Like the scenario observed with added mass, the influence of nacelle velocity on the aerodynamic damping becomes more pronounced at lower wind speeds. Specifically, when compared to the constant damping, the differences in aerodynamic damping values for the nacelle velocities of 0.1 m/s and 1.0 m/s amount to 5.4 % and 11.5 %, respectively, at a wind speed of 9.8 m/s. For the wind speed of 11.4 m/s, the differences in damping values corresponding to the minimum and maximum nacelle velocities are 16.3 % and 72.5 %, respectively. Therefore, in the vicinity of the rated wind speed and its immediate vicinity, the aerodynamic damping exhibits substantial frequency dependence and notable nonlinearity.

Fig. 7 presents the distribution of linear hydrodynamic damping to illustrate the significance of aerodynamic damping. It is observed that, for both surge and pitch responses, the hydrodynamic damping experiences a rapid reduction with increasing motion periods. For periods above 50 s, the hydrodynamic damping becomes negligible when compared with the aerodynamic damping. In such a case, when dealing with motion responses under low-frequency excitations, particular attention must be put to the inclusion of aerodynamic damping.

4. Motion response comparisons

This study specifically investigates scenarios in which wind, wave, and current are aligned in the 180 deg direction, focusing on surge and pitch responses. The tower base shear forces and bending moments of a fixed rotor serve as the external loads in the decoupled models. To assess the effects of aerodynamic damping on the motion responses, multiple aerodynamic damping models are employed, and the corresponding results are compared with those obtained from the coupled analyses.

4.1. Decoupled cases without aerodynamic damping

Figs. 8 and 9 present comparisons of surge and pitch responses between the coupled model and the decoupled model without the inclusion of aerodynamic damping. Overall, the effect of aerodynamic damping on surge motion falls within an acceptable range. Particularly in cases of severe sea states and near the cut-out wind speed (e.g., 21.7 m/s), the surge responses based on the coupled model are almost identical to those from the decoupled analysis. However, the absence of aerodynamic damping results in substantial differences in pitch responses. While the mean values remain consistent, noticeable differences are observed in the decoupled analyses.

In Fig. 10, the differences between the decoupled and coupled models are quantified in terms of maximum value and standard deviation. For surge responses, these relative errors are modest, i.e., the maximum values and the standard deviations respectively fall within 5 % and 10 %. The aerodynamic damping exerts a suppression effect on surge responses below rated wind speed. However, when the inflow wind speed reaches or exceeds the rated wind speed (e.g., 11.4 m/s, 13.0 m/s), the aerodynamic damping enhances surge responses, indicating the presence of "negative damping". For pitch responses, the relative errors are noticeable. In some instances, the standard deviation of decoupled analyses surpasses that of the coupled calculations by up to

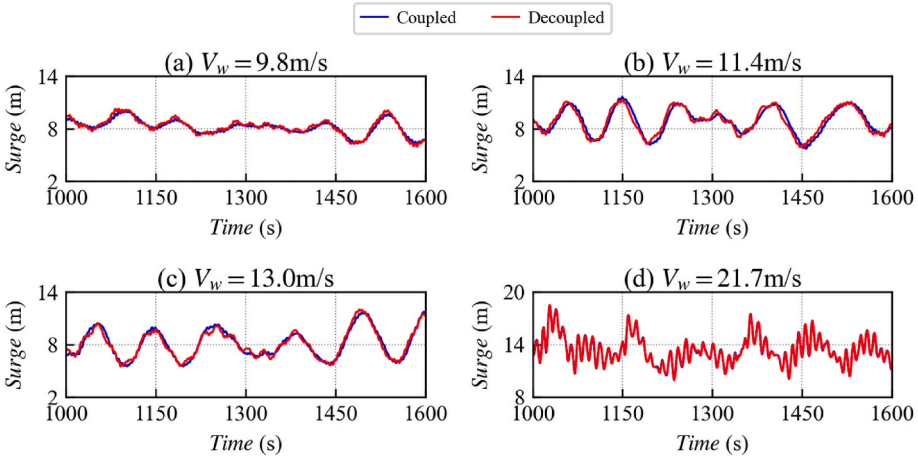

Fig. 8. Comparisons of surge responses between the coupled and decoupled models.

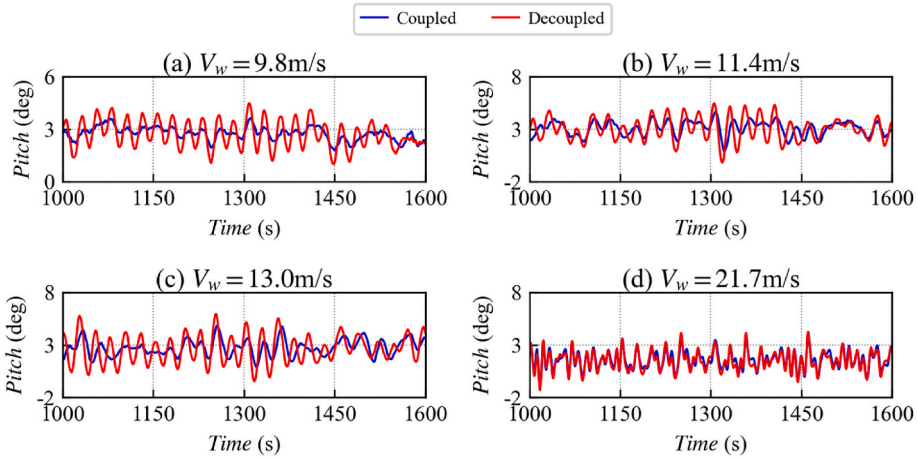

Fig. 9. Comparisons of pitch responses between the coupled and decoupled models.

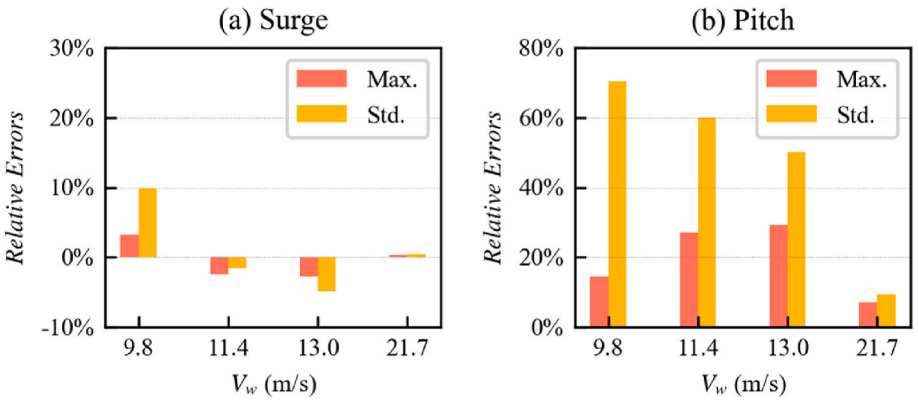

Fig. 10. Relative errors of the decoupled model compared with the coupled model.

70 %. For the case near the cut-out wind speed (21.7 m/s), the maximum and standard deviation errors remain below 10 % due to the minimal magnitude of aerodynamic damping.

To identify the sources of errors in decoupled analyses, Fig. 11 provides a comparison of power spectral densities (PSDs) of motion responses based on two different models. It is evident that the differences mainly exist in the natural frequency components. For surge responses, the decoupled model yields a spectral peak higher than that of the coupled model below rated wind speed. In contrast, at or above the rated wind speed, the spectral peak of the decoupled model is lower. Turning to pitch responses, the decoupled analyses result in noticeable natural frequency components in the spectral content. This implies that in the absence of aerodynamic damping, the natural frequency components of pitch responses remain unsuppressed, leading to considerable prediction errors.

The pitch responses exhibit a strong correlation with various crucial aspects such as power generation and nacelle safety. The above observation highlights the critical role of aerodynamic damping in accurately capturing the dynamics of pitch responses.

4.2. Decoupled cases with aerodynamic damping

To achieve the strategies for the selection of aerodynamic damping, we successively introduced constant damping and frequency-dependent damping (including added mass) into the decoupled models. It is important to emphasize that the aerodynamic damping exhibits not only frequency-dependent but also velocity-dependent characteristics. In our initial application, we employed aerodynamic damping and added mass with an oscillation velocity amplitude ωA of 0.1 m/s in decoupled models.

Figs. 12 and 13 respectively present the comparisons of surge and pitch responses. The legends "CstDp" and "FdDp" represent the results obtained using constant damping and frequency-dependent damping, respectively. In surge responses, the utilizing of constant damping in the decoupled model yields results closely aligned with the coupled analysis for wind speeds below the rated value and near cut-out value. However, at the rated and above-rated wind speeds, the surge response predictions with constant damping worsen. This degradation is attributed to the spurious natural frequency components of pitch. Conversely, cases with frequency-dependent damping exhibit surge responses that closely match the results of the coupled analyses, except at the rated wind speed condition, signifying significant improvements over simulations without damping or with constant damping. At the rated wind speed, the decoupled analysis results in maximum and standard deviation values 12.43 % and 54.39 % higher, respectively. As indicated in Fig. 6, the oscillation velocity amplitude exerts a notable influence on aerodynamic damping at the rated wind speed. This underscores the importance of accounting for the effect of oscillation velocity amplitude in decoupled analyses at rated wind speed.

Regarding pitch responses, the introduction of constant aerodynamic damping results in a favorable alignment between the decoupled and coupled analyses for below-rated wind speed. However, for wind speed at or above the rated value, noticeable amplification of natural frequency components of pitch occurs in the decoupled analyses. This is due to the aforementioned frequency-dependent aerodynamic damping. The aerodynamic damping is positive around the natural period of pitch.

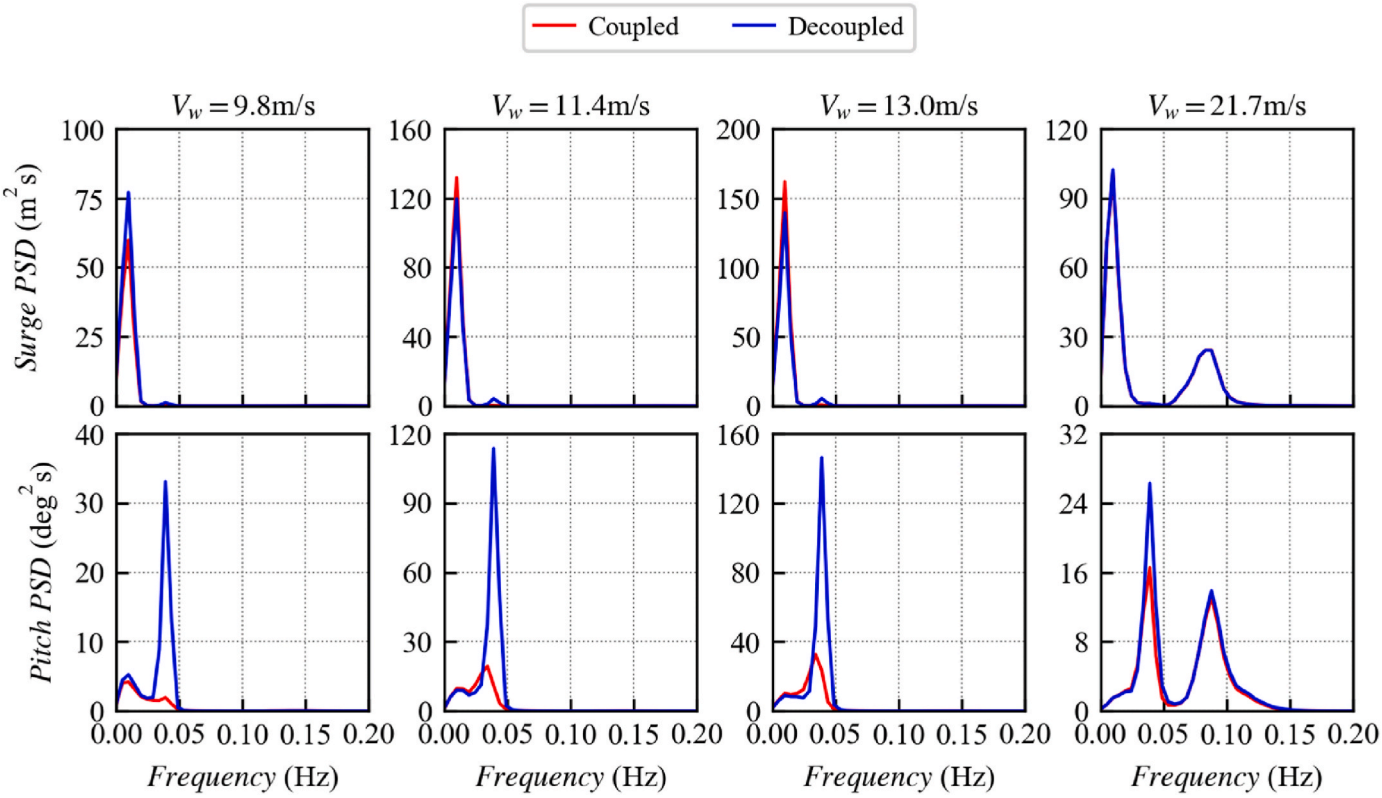

Fig. 11. PSD comparisons between the coupled and decoupled models without aerodynamic damping.

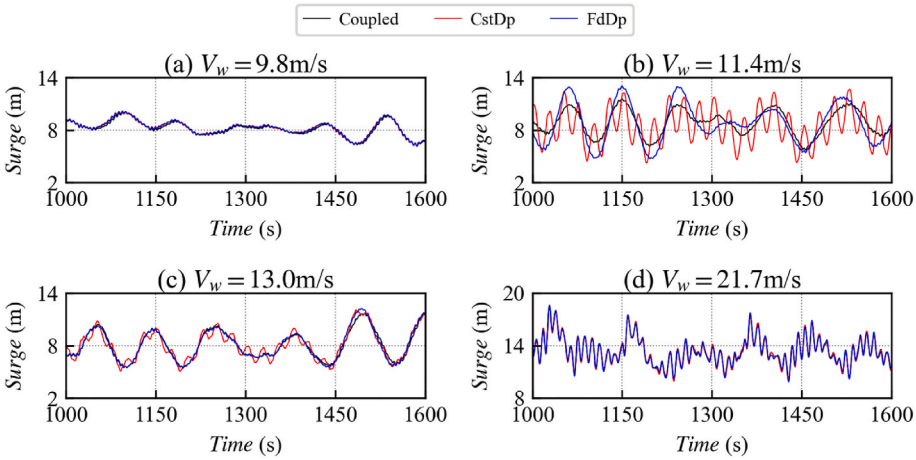

Fig. 12. Comparisons of surge responses between the coupled model and decoupled models with aerodynamic damping.

Thus, when simple negative constant damping is employed for rated or above-rated wind speeds, it would inevitably introduce unrealistic components. Cases utilizing frequency-dependent damping generally yield results closely aligned with the coupled analyses. Apart from that near cut-out wind speed condition, pitch responses exhibit substantial improvements when compared to simulations without damping or with constant damping. For the near-cut-out wind speed case, pitch responses from the decoupled model surpass those of the coupled analysis. This discrepancy is attributed to the negative value of aerodynamic damping near the natural period of pitch, and further investigations are needed to understand the occurrence of negative damping near the pitch's natural period for the near cut-out wind speed conditions.

Fig. 14 presents the PSDs of surge and pitch responses based on different models. In accordance with the time-domain results, the prediction errors of the constant damping models are primarily due to natural frequency components of the pitch motion, while the errors in the frequency-dependent damping models result from the assessment of the aerodynamic damping at rated wind speed and the occurrence of negative damping around the natural frequency of the pitch motion, for the near-cut-out wind speed condition.

4.3. Decoupled cases with frequency- and velocity-dependent aerodynamic damping

In light of the considerable influence of oscillation velocity on the aerodynamic damping for rated wind speed, we have conducted decoupled analyses utilizing aerodynamic damping corresponding to varying oscillation velocities for rated wind speed case.

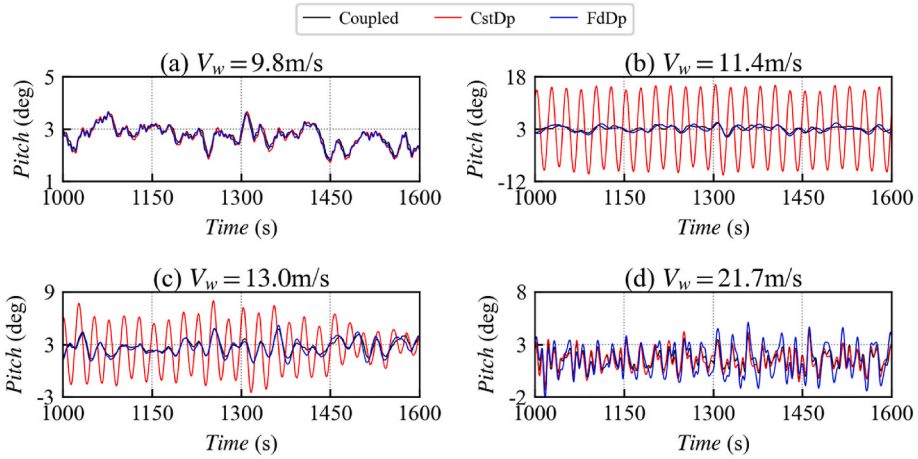

Fig. 13. Comparisons of pitch responses between the coupled model and decoupled models with aerodynamic damping.

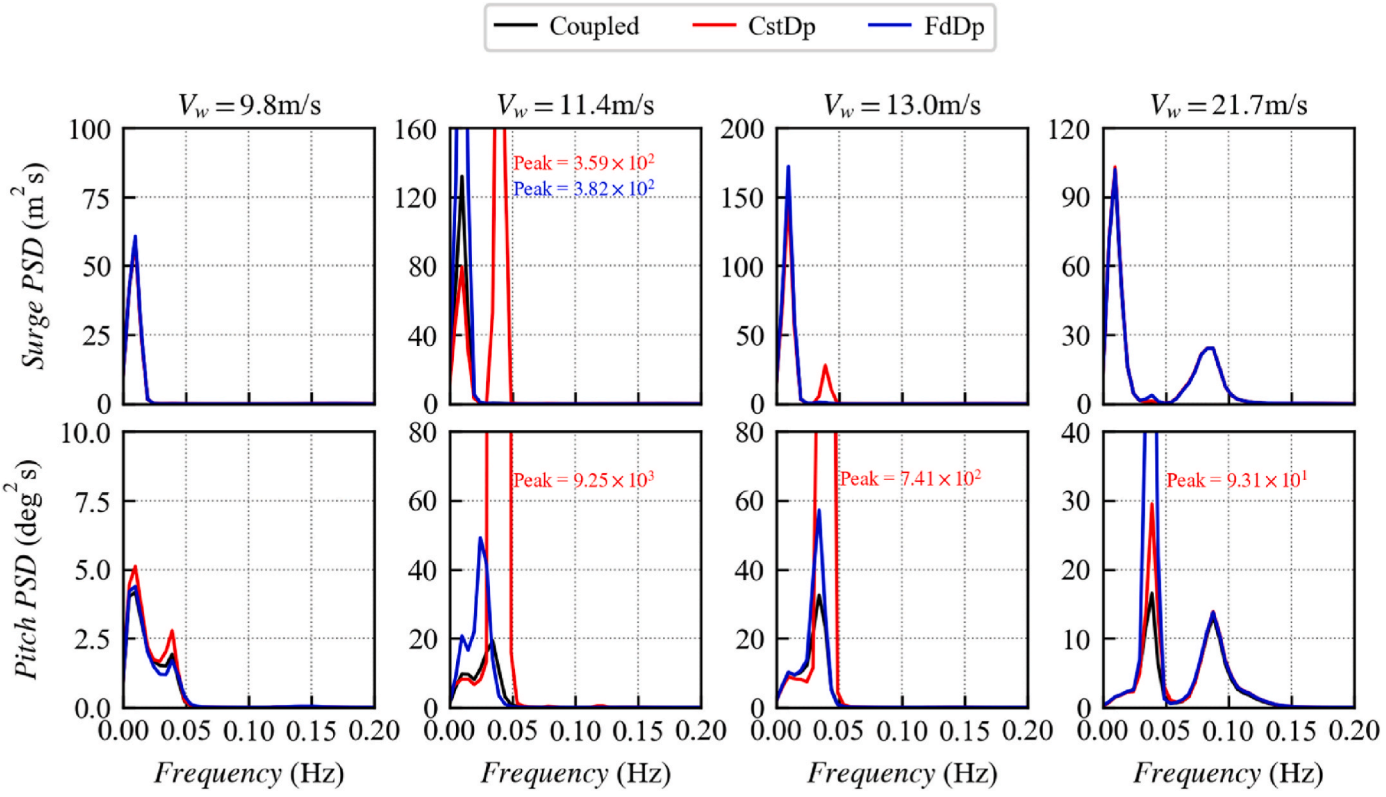

Fig. 14. PSDs comparisons between the coupled and decoupled models with aerodynamic damping.

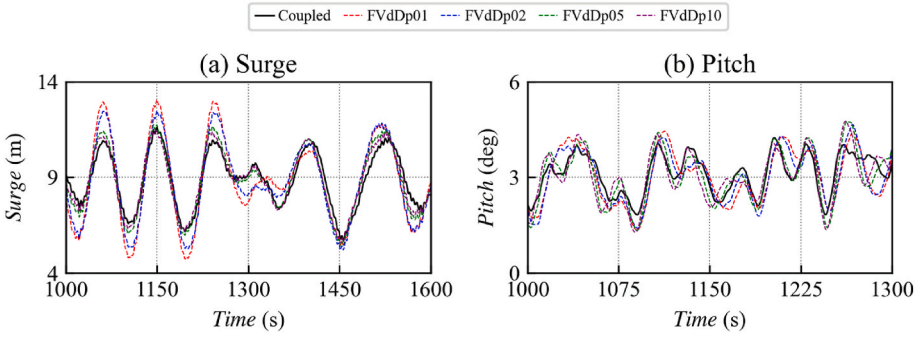

Fig. 15. Surge and pitch responses for coupled and decoupled models (Frequency-velocity-dependent damping and added mass included in the decoupled models).

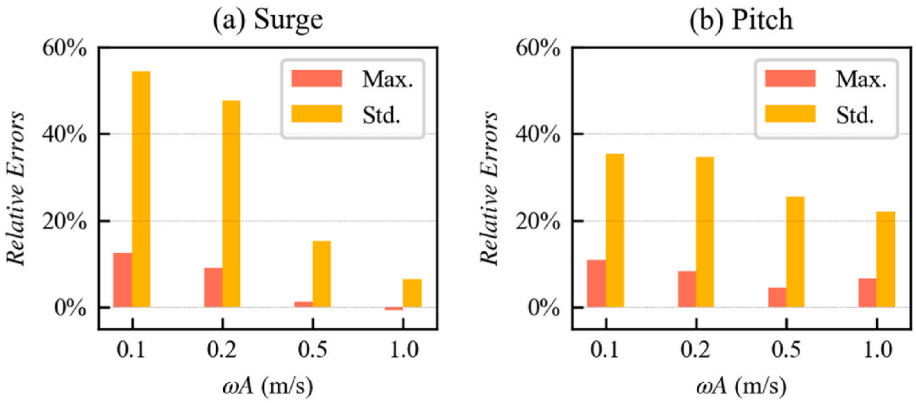

Fig. 16. Relative errors of the decoupled models compared with the coupled models.

Fig. 15 presents the surge and pitch responses for both the coupled model and the decoupled models with different levels of aerodynamic damping. The numbers occur in legends, i.e. '01′, '02′, '05′ and '10', correspond to the ωA in Fig. 6(b). Fig. 16 quantifies relative errors between these modeling approaches. It shows that as the oscillation velocity amplitude (ωA) increases, the surge response approaches the results from the coupled analysis. In particular, when attains 1.0 m/s, the relative errors for the maximum value and standard deviation of the surge responses are −0.72 % and 6.41 %, respectively. Similar trends associated with the oscillation velocity amplitude are observed in pitch responses. That is, it tends to converge with the results of the coupled analysis as the oscillation velocity amplitude increases. Further scrutiny of the relative wind speed variance in the coupled analysis reveals a standard deviation of approximately 0.4 m/s for nacelle fore-aft velocity and around 1.6 m/s for turbulent wind. This emphasizes that in conditions near or at rated wind speed, the determination of frequency-dependent aerodynamic damping should factor in relative velocity fluctuations stemming from both the nacelle fore-aft displacement and turbulent wind.

To demonstrate the computational efficiency advantages of the decoupled methodology, benchmark tests were executed on an AMD Ryzen @ 2.10 GHz laptop for this 11.4 m/s wind speed scenario. Under identical modeling conditions, including matching floater and mooring configuration, time step of 0.1 s, implicit integration algorithms, and a 3-h simulation duration, the coupled simulation required 37 min, while the decoupled approach consistently achieved results in 21 min, representing a 43 % reduction in computational time. Critically, the magnitude of efficiency gains is tightly related to node counts in turbine blade/tower structures and mooring discretization.

5. Conclusions

To accurately and efficiently evaluate the motion responses of FOWTs, this study conducted decoupled analyses using constant, frequency-dependent, and frequency-velocity-dependent aerodynamic damping models. The results were compared with those from coupled analyses. The main conclusions are as follows:

(1) The effect of aerodynamic damping on surge motion is relatively modest. However, at or above the rated wind speed, the occurrence of 'negative damping' amplifies the surge responses. In contrast, aerodynamic damping significantly suppresses pitch motion, and neglecting it results in substantial overestimations of pitch response.
(2) Constant aerodynamic damping improves the accuracy of pitch responses under below-rated wind speed conditions. However, for rated and above-rated wind speeds, the application of constant aerodynamic damping results in more pronounced prediction inaccuracies.
(3) Incorporating frequency-dependent aerodynamic damping in decoupled models yields surge and pitch responses that generally align well with the results of coupled analyses.
(4) It is crucial to account for the effect of oscillation velocity amplitude when considering frequency-dependent aerodynamic damping in decoupled models at rated wind speed.

These findings serve as valuable guidance for engineering design and analysis of FOWTs. It shows that using pre-calculated wind loads without considering frequency-dependent aerodynamic damping may result in substantial errors in practical design.

CRediT authorship contribution statement

Yanfei Deng: Writing – original draft, Methodology, Formal analysis, Conceptualization. **Sara Ying Zhang:** Investigation, Data curation. **Yifeng Yang:** Writing – review & editing, Visualization, Methodology. **Bingfu Zhang:** Writing – review & editing. **Yifei Wang:** Visualization. **Jiahao Chen:** Writing – review & editing. **Weiping Hou:** Validation, Software.

Declaration of competing interest

The authors declare that they have no known competing financial interests or personal relationships that could have appeared to influence the work reported in this paper.

Acknowledgment

This work was financially supported by National Natural Science Foundation of China (52301317), Guangdong Basic and Applied Basic Research Foundation (2024A1515011587), Shenzhen Science and Technology Program (JCYJ20240813110411016), the Guangdong Provincial Department of Science and Technology's Guangdong-Hong Kong-Macao Joint Innovation Project (No. 2024A0505040006) and Guangdong Provincial Special Funds for Marine Economic Development (GDNRC[2023]48). These sources of support are gratefully acknowledged.

References

Alexandre, A., Antonutti, R., Gentils, T., Mutricy, L., Weyne, P., 2021. Simplified aerodynamic loading model for non-production conditions for floating wind systems design. In: The Third International Offshore Wind Technical Conference. American Society of Mechanical Engineers, V001T002A001. Virtual, Online.
Beshbichi, O.E., Xing, Y., Ong, M.C., 2021. An object-oriented method for fully coupled analysis of floating offshore wind turbines through mapping of aerodynamic coefficients. Mar. Struct. 78, 102979.

Chen, C., Duffour, P., Fromme, P., 2020. Modelling wind turbine tower-rotor interaction through an aerodynamic damping matrix. J. Sound Vib. 489, 115667.
Chen, C., Duffour, P., Fromme, P., Hua, X., 2021. Numerically efficient fatigue life prediction of offshore wind turbines using aerodynamic decoupling. Renew. Energy 178, 1421–1434.
Chuang, T.-C., Yang, W.-H., Yang, R.-Y., 2021. Experimental and numerical study of a barge-type FOWT platform under wind and wave load. Ocean Eng. 230, 109015.
Coulling, A.J., Goupee, A.J., Robertson, A.N., Jonkman, J.M., Dagher, H.J., 2013. Validation of a FAST semi-submersible floating wind turbine numerical model with DeepCwind test data. J. Renew. Sustain. Energy 5 (2), 023116.
Deng, Y., Zhang, S.Y., Zhang, M., Gou, P., 2023. Frequency-dependent aerodynamic damping and its effects on dynamic responses of floating offshore wind turbines. Ocean Eng. 278, 114444.
DNV·GL, 2018a. DNVGL-ST-0119: Floating Wind Turbine Structures. DNV GL.
DNV·GL, 2018b. DNVGL-ST-0437: Loads and Site Conditions for Wind Turbines. DNV·GL.
Foxwell, D., 2022. Eel-Like Foundation for Floating Windfarms Is Ideal for Mass Production. Riviera Maritime Media Ltd.. Online.
Ghigo, A., Cottura, L., Caradonna, R., Bracco, G., Mattiazzo, G., 2020. Platform optimization and cost analysis in a floating offshore wind farm. J. Mar. Sci. Eng. 8 (11), 835.
IEC, 2019. Wind Energy Generation systems-part 3-2: Design Requirements for Floating Offshore Wind Turbines. International Electrotechnical Commission, Geneva, Switzerland, pp. 61400–61403.
Jonkman, J.M., 2007. Dynamics Modeling and Loads Analysis of an Offshore Floating Wind Turbine. University of Colorado at Boulder.
Karimirad, M., Moan, T., 2012. A simplified method for coupled analysis of floating offshore wind turbines. Mar. Struct. 27 (1), 45–63.
Lerch, M., De-Prada-Gil, M., Molins, C., 2018. A simplified model for the dynamic analysis and power generation of a floating offshore wind turbine. E3S Web Conf. EDP Sci., 00001
Ma, Y., Chen, C., Fan, T., Lu, H., 2022. Research on the dynamic behaviors of a spar floating offshore wind turbine with an innovative type of mooring system. Front. Energy Res. 10, 203.
Matha, D., Sandner, F., Schlipf, D., 2014. Efficient critical design load case identification for floating offshore wind turbines with a reduced nonlinear model. J. Phys. Conf. 555 (1), 012069.
Pegalajar-Jurado, A., Borg, M., Bredmose, H., 2018. An efficient frequency-domain model for quick load analysis of floating offshore wind turbines. Wind Energ. Sci. 3 (2), 693–712.
Rixen, D.J., Valk, P.L.C.v.d., 2013. An impulse based substructuring approach for impact analysis and load case simulations. J. Sound Vib. 332 (26), 7174–7190.
Riyanto, R.D., Papadopoulos, J.M., Myers, A.T., 2022. Numerical investigation of wave following mechanism of shallow draft floating wind turbine. In: International Conference on Offshore Mechanics and Arctic Engineering. American Society of Mechanical Engineers, V001T001A017.
Robertson, A., Jonkman, J., Masciola, M., Song, H., Goupee, A., Coulling, A., Luan, C., 2014. Definition of the Semisubmersible Floating System for Phase II of OC4. National Renewable Energy Laboratory (NREL), Golden, CO (United States).
Souza, C.E.S., Bachynski, E.E., 2019. Changes in surge and pitch decay periods of floating wind turbines for varying wind speed. Ocean Eng. 180, 223–237.
Souza, C.E.S., Hegseth, J.M., Bachynski, E.E., 2020. Frequency-dependent aerodynamic damping and inertia in linearized dynamic analysis of floating wind turbines. J. Phys. Conf. 1452 (1), 012040.
Subbulakshmi, A., Verma, M., Keerthana, M., Sasmal, S., Harikrishna, P., Kapuria, S., 2022. Recent advances in experimental and numerical methods for dynamic analysis of floating offshore wind turbines—An integrated review. Renew. Sustain. Energy Rev. 164, 112525.
Tucker, M.J., Pitt, E.G., 2001. Waves in Ocean Engineering.
Valamanesh, V., Myers, A.T., 2014. Aerodynamic damping and seismic response of horizontal axis wind turbine towers. J. Struct. Eng. 140 (11), 04014090.
Xi, R., Wang, P., Du, X., Xu, K., Xu, C., Jia, J., 2020. A semi-analytical model of aerodynamic damping for horizontal axis wind turbines and its applications. Ocean Eng. 214, 107861.
Yang, J., He, Y.-P., Zhao, Y.-S., Shao, Y.-L., Han, Z.-L., 2021. Experimental and numerical studies on the low-frequency responses of a spar-type floating offshore wind turbine. Ocean Eng. 222, 108571.
Yang, X., Bai, X., Cao, H., 2022. Influence analysis of rime icing on aerodynamic performance and output power of offshore floating wind turbine. Ocean Eng. 258, 111725.
Yang, Y., Bashir, M., Michailides, C., Li, C., Wang, J., 2020. Development and application of an aero-hydro-servo-elastic coupling framework for analysis of floating offshore wind turbines. Renew. Energy 161, 606–625.